Microscopic characterization of InAs/$In_{0.28}GaSb_{0.72}$/InAs/AlSb laser structure interfaces

W. Barvosa-Carter,* M. E. Twigg, M. J. Yang, and L. J. Whitman†
Naval Research Laboratory, Washington, Washington, D.C. 20375
(Received 26 January 2001; published 4 June 2001)

We have used cross-sectional scanning tunneling microscopy (XSTM) and transmission electron microscopy (TEM) to study InAs/$In_{0.28}Ga_{0.72}$Sb/InAs/AlSb strained-layer heterostructures designed for use in infrared lasers. The samples came from the same material previously characterized by photoluminescence (PL) and x-ray diffraction [M. J. Yang *et al.*, J. Appl. Phys. **86**, 1796 (1999)]. Several structures grown at different temperatures and with either III-As or III-Sb-like interfacial bonds have been characterized. Analysis of high-resolution TEM images finds the same degree of interfacial roughness (~1 ML) for both III-As and III-Sb interfacial bonded heterostructures, despite significantly greater PL intensity in the latter. We also implement and compare two different methods for analyzing the interfacial roughness using XSTM; both show that the crucial InAs/InGaSb interface is rougher in the samples grown at high temperature. Even in samples grown at the optimal temperature (~440 °C), XSTM reveals intermixing at the AlSb-on-InAs interfaces, as well as unexpected differences in the interfacial bond types at the InAs-on-AlSb vs AlSb-on-InAs interfaces. Whereas all layers grown at or below the optimal growth temperature appear defect-free in TEM, threading dislocations are observed in samples grown at higher temperature.

DOI: 10.1103/PhysRevB.63.245311 PACS number(s): 68.37.−d, 68.55.Ln, 68.65.Cd

I. INTRODUCTION

Considerable research on midwavelength (3–5 μm) and long-wavelength (8–14 μm) infrared (IR) diode lasers is being driven by both military and commercial demand for high output power and noncryogenic operation.[1–3] Molecular beam epitaxy (MBE) has allowed the creation of novel lasing materials, new lasing transitions, and record-setting performances for devices operating in these wavelength ranges.[4–6] However, in order to optimize these devices, control over mesoscale and nanoscale defects in the material must be achieved. The strain in the heterolayers, for instance, can lead to strain-driven roughening of the growth surface and the introduction of misfit and threading dislocations. At the nanometer scale, precise control over layer thickness must be maintained, because even *monolayer-scale* roughness and interdiffusion between the composite layers in the heterostructures can cause degradation in device efficiency and performance.[7,8] Because very little information is currently available concerning such defects in actual device structures, their characterization should hasten further improvements of the device material.

In this article, we report our investigations of the nanoscale and mesoscale structural properties of InAs/InGaSb/InAs/AlSb superlattices designed for ''W-structure'' mid-IR lasers.[9] A qualitative sketch of the spatially varying band gaps and offsets is given in Fig. 1(a). The electron-hole recombination process that leads to lasing takes place across the InAs/InGaSb interfaces, making these the most critical interfaces in the structure. The primary function of the AlSb layer is to confine the electrons and holes in the InAs/InGaSb/InAs layers, and to suppress the formation of extended three-dimensional electron states between neighboring sets of InAs layers. The AlSb/InAs interfaces and the quality of the AlSb layer are therefore deemed less critical to optimizing the lasing process, although defects in and conductive pathways through the AlSb layer would certainly be deleterious to device performance.

The photoluminescence (PL) and double-crystal x-ray diffraction (XRD) of these laser structures are strongly dependent on MBE growth temperature.[10,11] As shown in Fig. 1(b),

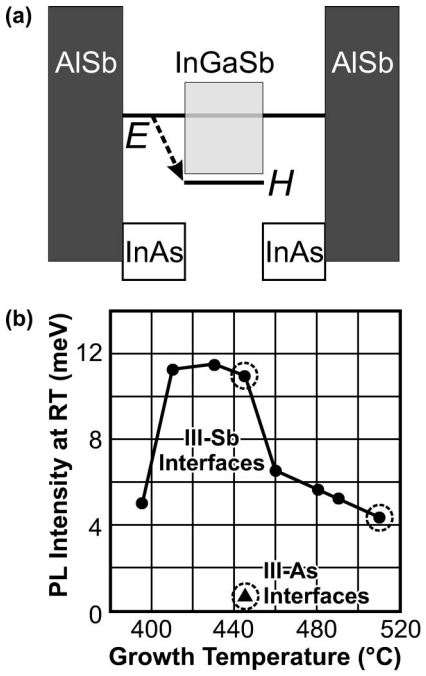

FIG. 1. (a) Composition and band offsets for the W-type laser structures evaluated in this work. The boxes represent the band gaps of the different material layers. Carrier recombination leading to light emission occurs between quantum-confined electron levels in the InAs layers (E) and heavy- and light-hole bands in InGaSb (H). (b) Integrated photoluminescence intensity at room temperature for samples grown at various temperatures with either III-Sb or III-As interfacial bonds (Ref. 11). The samples characterized in this study are circled.

the optical characteristics are optimal within a rather narrow growth temperature range (410–450 °C), and are typically much worse outside of that range. In addition, the inclusion of III-As vs III-Sb-like interfacial bonds between the InAs and InGaSb layers drastically affects the material quality as measured by PL, but appears to leave the macroscopic structural quality unchanged as measured by XRD.[10,11] The goal of this work is to understand the source of the dependence of material quality on temperature and bond type, and to identify the defects occurring in the material under various growth conditions. We attempt to directly correlate the atomic-scale and mesoscale properties of the material, such as dislocation density and interfacial roughness, with growth conditions and macroscopic properties, by studying samples of the *same material* previously characterized by PL and XRD. To characterize the properties of the layers and interfaces over a range of length scales, we used a combination of transmission electron microscopy (TEM) and atomic-resolution cross-sectional scanning tunneling microscopy (XSTM).

Whereas TEM is well developed and widely implemented for characterization of electronic devices, XSTM is generally less familiar for this application. It is a potentially powerful technique for imaging defects in superlattice structures, where one uses STM to image a {110} cleavage face of a piece of superlattice material, allowing ''edge-on'' cross-sectional characterization of the as-grown superlattice. In particular, XSTM can obtain *atomic-scale* information about the superlattice layers and interfaces, although it has some limitations that have only recently been explored in detail.[12] One limitation of particular relevance to this work is the fact that only every other atomic layer in the superlattice can be imaged. Here we will also describe the impact of this limitation on our ability to adequately quantify interfacial roughness.

II. EXPERIMENT

The samples studied here came from superlattices grown and previously characterized by a variety of techniques.[10,11,13] Briefly, the ''W'' structures were grown on GaSb substrates in an MBE chamber equipped with a valved As cracker, an Sb cracker, and a conventional Sb effusion cell. The buffer layer consisted of 0.3 μm of GaSb grown at 530 °C followed by 1.0 μm of AlSb grown at 580 °C. The substrates were then cooled without Sb_2 flux to a lower temperature for superlattice growth. The four-constituent ''W'' active layer consisted of 20 periods of 5.5 ML InAs/10-ML $In_{0.28}Ga_{0.72}Sb$/5.5-ML InAs/14-ML AlSb. Subsequently, a capping layer consisting of 0.2 μm of AlSb and 10 nm of GaSb was grown at 480 °C. Active layers were grown at a variety of temperatures with either InSb or GaAs interfacial bonds.[10,11]

High-resolution TEM (HRTEM) of cross-sectional TEM (XTEM) samples was performed by imaging along the [001] direction through the corner of cleaved samples.[14] Other XTEM samples were prepared by mechanical lapping followed by ion milling at liquid-nitrogen temperature. Micron-scale features such as threading dislocations were examined by imaging cleaved plan-view samples with the incident electron beam directed 45° from the growth direction. As described in detail elsewhere,[12] XSTM samples scribed from the same wafers were mounted on an STM sample holder. After introducing the samples into the STM vacuum chamber, a sample was then scribed *in situ* and cleaved to expose either a (110) or $(\bar{1}10)$ surface. Single-crystal tungsten tips were prepared by electrochemical etching and cleaned *in situ* by electron-bombardment heating prior to use. All constant-current images shown are of filled states on (110) surfaces unless otherwise noted.

III. RESULTS AND DISCUSSION

A. Interfacial roughness

To understand the effect of growth temperature on the atomic-scale structure of the material, we have used XSTM to compare several laser structures with InSb interfacial bonds: one grown at the optimal temperature (based on PL) and another grown at higher temperature. [The samples studied are circled in Fig. 1(b)]. Here we wish to distinguish between two sources of interfacial disorder: (1) roughness, as might arise from incomplete layer completion during epitaxy and (2) interlayer mixing at the InAs/InGaSb/InAs interfaces. Figure 2 compares XSTM images from the (110) faces of the two cleaved superlattices (optimal vs higher temperature). Both samples were grown on the same day using otherwise identical conditions. Close examination of the images shows that roughness at the crucial InAs/InGaSb interface appears to be somewhat larger at the higher growth temperature. In addition, the InGaSb-alloy layers appear less uniform in the high-temperature samples. In this section, we will focus on characterizing the roughness of the interfaces.

To obtain a quantitative measurement of this roughness, we have followed and extended the methods of Feenstra and co-workers[15–17] and Harper *et al.*[18,19] Interface profiles are typically extracted from an STM image by first taking a derivative of the image and then extracting the interface profile by tracing a contour of constant slope. This method can result in a reasonable facsimile of the interface profile provided the individual surface atoms are not well resolved and there is sufficient image contrast between the layers. However, the approach becomes difficult to implement when the surface atoms are well resolved. In this case, one can extract interface profiles from individual images by hand, by manually inspecting each atom in the image and determining which layer it belongs to based on its height in the STM image. Although the height is largely determined by the identity of the surface atom (e.g., Sb vs As), the presence of an alloy can confuse this method because the identity of the subsurface atoms (In or Ga, randomly determined by the alloy composition) can also affect the height.[20,21] The effect on the measured height is greatest for the first subsurface layer, with deeper layers contributing successively less. The net effect is to make the heights of the atoms in the alloy appear highly irregular. This variability is particularly pronounced at an interface, because the interfacial bond type (i.e., long Sb-like

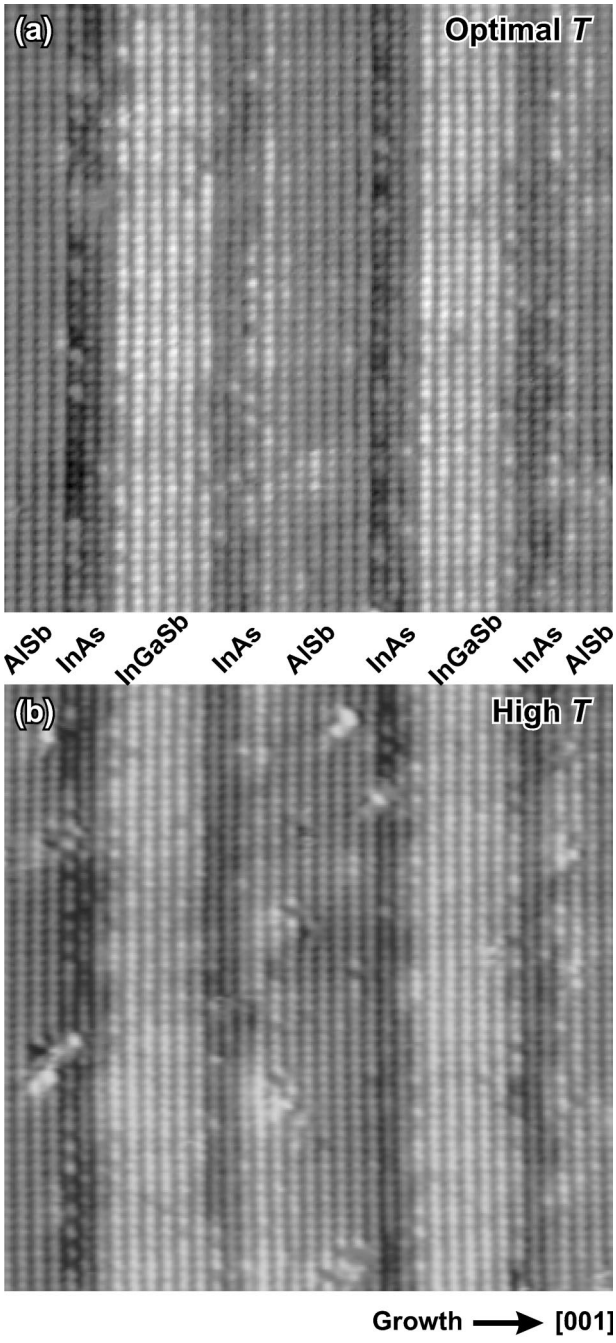

FIG. 2. Atomic-resolution XSTM images (23×23 nm) of two laser structure samples grown with nominal III-Sb interfacial bonds at (a) the optimal temperature (as measured by PL) and (b) at high temperature. The sample biases and tunneling currents were (a) -2.0 V, 50 pA and (b) -2.0 V, 0.1 nA.

bonds vs shorter As-like ones) can enhance the alloy effects and hinder unambiguous determination of the interface profile.[12,22]

In order to avoid the subjective assessment required to visually trace each interface and to additionally enable the rapid analysis of multiple images, we have developed an alternate approach to tracing the interface profiles. As illustrated in Fig. 3, we start with an image at a resolution of about 5 pixels per unit cell along the interface. We then

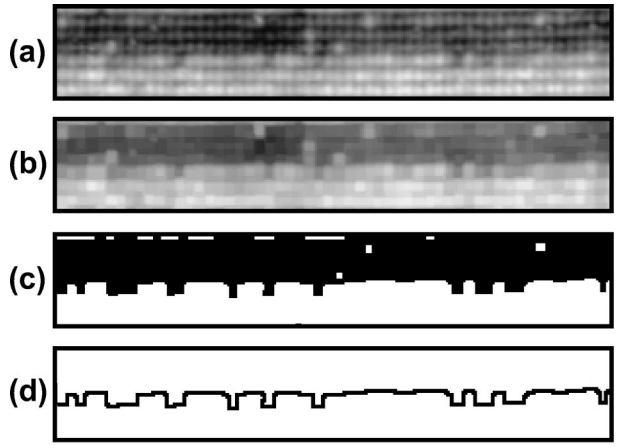

FIG. 3. Sequence of images illustrating the processing steps used to extract interface profiles from the XSTM images. (a) Original gray-scale image, -2 V, 0.1 nA (at least 5 pixels per surface unit cell along the interface). (b) Image after twice replacing each pixel with the minimum value of its 3×3 kernel, and then replacing each pixel with the 3×3 maximum. (c) Two-color image with threshold midway between the average values of the two layers. (d) The interface defined by simple edge detection.

smoothen the image using a 3×3-pixel window, and then reduce it to black and white using a threshold value midway between the average pixel intensities on either side of the interface. Finally, the profile of the interface is extracted from the two-color image using simple edge detection. Because the contrast in each image is normalized and each image is treated to the same sequence of manipulations, the interface definition is unique across the entire set of data and all surface atoms are treated on a consistent basis. When implementing this method, it is useful to oversample the interface profile, i.e., to use more data points than atomic positions along the interface. Oversampling helps take into account those surface atoms that, due to alloy or interface-stoichiometry effects, have a topographic height intermediate between the bulk layers on either side. When analyzing power spectra from the oversampled interface profile, however, the power spectral density for wavevectors above the Nyquist limit defined by the surface unit cell mesh must be excluded from subsequent analysis.[23]

The interfacial power spectrum can be directly obtained from a fast-Fourier transform (FFT) of the interface profile. The associated power spectral density can be very accurate if the imaged interfacial roughness extends over multiple layers. However, because only every other layer of the crystal is imaged, if the roughness includes only two or three growth layers, this method can lead to errors: a significant portion of the roughness may be obscured between observed atomic layers.[12] To examine the potential impact of this problem, we have analyzed our interface profiles that fall into this category using two techniques: the usual method of Feenstra and co-workers,[15–17] which we will denote as the ''direct'' method, and a modification of this approach, which we will call the ''inspection'' method. When implementing the direct method, we treat all interface measurements in units of the {110}-row spacing, 6.1 Å (corresponding to 2 ML during

epilayer growth). Power spectra from *all* interfaces, including ones with near-zero rms roughness, are averaged when determining the final power spectra. In contrast, within the inspection method, we deliberately *exclude* interface profiles from the analysis that exhibit near-zero rms roughness, i.e., those where it appears that the actual interface is hidden from observation. Furthermore, for cases where the interface is visible across a single row on the {110} surface, we treat the observed roughness in units of 3.05 Å (the growth monolayer height). This makes physical sense because steps and islands on the (001) growth surface are virtually always this high.[12]

The roughness of the exposed cleavage surface typically increases towards the capping layer, so that finding portions of the superlattice long enough for analysis becomes more difficult farther away from the buffer layer. Hence, we have limited our XSTM study to the interfacial roughness of the first three to four superlattice periods out of the 20 grown. From these segments of the superlattice, we have extracted nearly 100 interface profiles of length ~215 Å from numerous atomic-resolution images (51 surface unit cells sampled at 5 data points per unit cell).[24] We then obtained the power spectral density from each using an FFT power-spectral density estimator with Welch windowing.[25] The power spectra for a particular interface—e.g., the InAs-on-InGaSb interface for the optimal temperature sample—were then averaged and fit to the usual Lorentzian power-spectral density plus an additional background term,

$$|A_q|^2 L = \frac{2\Delta^2 \Lambda}{[1+(q\Lambda)^2]} + B^3, \tag{1}$$

where A_q is the Fourier amplitude at wavevector q, L is the length of the interface profiles, Δ is the roughness amplitude, Λ is the correlation length, and B represents the ''white noise'' component arising from uncorrelated point defects.[18,19]

In Fig. 4, we show the power spectra extracted using the direct method for the InAs-on-InGaSb and InGaSb-on-InAs interfaces for both the optimized (a) and high-temperature (b) samples. The data have been fit to Eq. (1) with (solid line) and without (dashed) the white noise background term B. The averaged power spectra extracted for both sample sets using both the direct and inspection methods are shown in Fig. 4(c), along with the Lorentzian fits (without the white noise term). The results of the fitting are summarized in Table I.

Comparing the results for the direct vs inspection method, we expect the direct method to overestimate the magnitude of the actual interfacial roughness, and indeed we find that to be the case: it finds a larger roughness by a factor of ~1.5. We also find that the length scale of the roughness is the same for both methods—this should generally be true if the interfacial roughness does indeed only extend over 2 ML. For larger excursions, the inspection method will find a length scale that is too short and the direct method becomes more accurate. In general, when the roughness extends over more than 2 ML, the direct method should be more accurate for quantifying the interfacial roughness.

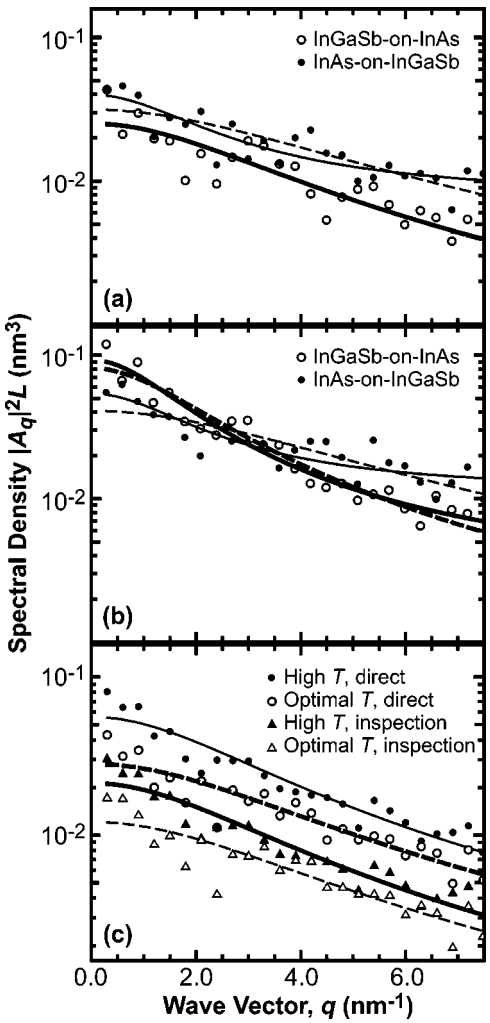

FIG. 4. Average power-spectral densities (PSD's) for the interfacial roughness obtained for various III-Sb interfaces, samples, and analysis methods. (a) Results for the optimal temperature sample for profiles extracted by the ''direct method'' for the InGaSb-on-InAs and InAs-on-InGaSb interfaces. Fits to Eq. (1) with (solid lines) and without (dashed lines) the optional white noise parameter B are included. Note that the InGaSb-on-InAs fit is the same with or without inclusion of white noise. (b) The same analysis for the high-temperature sample. (c) Comparison of the overall interfacial roughness (given by an average of PSD's for both interfaces) for the optimal- and high-temperature samples, fit without the white noise parameter.

Two striking features arise from the analysis. First, we find that the interfacial roughness in the high-growth-temperature structure is indeed significantly larger than in the structure grown at the optimal temperature by 0.4–0.7 Å rms (depending on the method used). Second, although we find asymmetries between the InAs-on-InGaSb and InGaSb-on-InAs interfaces, they all share a remarkably short correlation length, 2–6 Å. The magnitude of the correlation length, Λ, for both samples is similar regardless of the power-spectrum extraction method used or the interface type (InAs-on-InGaSb or InGaSb-on-InAs). This similarity indicates that the structure of the growth surface does not change significantly over the ~50 °C growth-temperature span used.

TABLE I. Fitting parameters for the Lorentzian power-spectral densities plotted in Fig. 4.

	Roughness Δ (Å)	Correlation length λ (Å)	White noise B (Å)
InGaSb-on-InAs, optimal T	2.01 ± 0.06	3.10 ± 0.36	
InGaSb-on-InAs, optimal T	2.00 ± 0.26	3.11 ± 0.83	0.01 ± 2.20
InAs-on-InGaSb, optimal T	2.62 ± 0.08	2.28 ± 0.26	
InAs-on-InGaSb, optimal T	1.83 ± 0.20	4.78 ± 1.30	7.78 ± 1.93
InGaSb-on-InAs, high T	2.91 ± 0.07	4.78 ± 0.37	
InGaSb-on-InAs, high T	2.73 ± 0.11	5.99 ± 0.78	2.71 ± 1.21
InAs-on-InGaSb, high T	3.02 ± 0.08	2.23 ± 0.24	
InAs-on-InGaSb, high T	2.02 ± 0.20	5.20 ± 1.35	11.22 ± 2.18
Direct, optimal T	2.29 ± 0.05	2.68 ± 0.23	
Inspection, optimal T	1.51 ± 0.04	2.64 ± 0.25	
Direct, high T	2.90 ± 0.06	3.33 ± 0.23	
Inspection, high T	1.81 ± 0.04	3.23 ± 0.23	

We also find that the accuracy of the fit (as measured by χ^2) for the InGaSb-on-InAs interfaces does not improve significantly when the background term is added, resulting in an insignificant background contribution. In contrast, the fits do improve for the InAs-on-InGaSb interfaces if this term is included, resulting in $\sim$30% smaller roughness Δ and roughly doubled correlation length Λ.

The simplest interpretation of the roughness results is that the interface is best characterized as a combination of random, short-range correlated clusters. Such clusters could arise from either diffusive or anion-exchange related processes between the heterolayers, or reconstruction-related stoichiometry changes during interface formation. Close inspection of the interface profiles reveals this behavior in real space: when observable, the interface is primarily composed of closely spaced but isolated or paired Sb or As atoms. Hence, the main effect of high growth temperature on the InAs/InGaSb/InAs interfaces is to simply increase the rms roughness of the interface.

The strikingly short correlation lengths we observe, relative to the findings of Lew *et al.*[26] and Feenstra and co-workers,[15–17] suggest a simple mechanism for the generation of interfacial roughness in these structures that is directly related to the use of MEE to form the interfaces. Each InGaSb-on-InAs interface in these samples was formed by terminating the InAs layer with a monolayer of In followed by an Sb soak. The In layer is intended to prevent Sb-As exchange and to force InSb interfacial bonds. A residual effect of this procedure is that the $\sim\frac{1}{2}$ ML of As terminating the InAs(001)-(2×4) reconstruction must be filled in by Sb.[12,27,28] In cross section, this would appear as short-correlated clusters of As and Sb as observed. To form the InAs-on-InGaSb interface, a monolayer of In was also deposited on the Sb-terminated InGaSb surface to force InSb bonding. It has been observed that 0.6–0.7 ML of the Sb from the terminal InGaSb surface can segregate into the subsequently deposited InAs.[29] Hence, a significant amount of Sb will be incorporated into the first InAs layers grown on top of the InGaSb layer. A short correlation length for these Sb atoms is certainly to be expected, because the diffusion length of group-V atoms on anion-terminated surfaces is generally accepted to be small.

Contrary to prior studies of interfacial roughness in InAs/InGaSb heterostructures, we find only slight differences between the InAs-on-InGaSb and InGaSb-on-InAs interfaces for either the sample grown at 410 or 450 °C. Lew *et al.*[26] found that the InAs-on-InGaSb interfaces were significantly rougher than the InGaSb-on-InAs ones in $In_{0.25}Ga_{0.75}Sb$/InAs superlattices grown at 380 °C. In contrast, Feenstra and co-workers[15–17] observed the reverse to be true for InAs/GaSb multilayers grown at 380 °C: their InAs-on-GaSb interfaces were found to be smoother than GaSb-on-InAs interfaces. They explained this behavior based on the thermodynamics of Sb segregation on InAs. However, they also observed that the asymmetry gradually disappeared as surface diffusion during growth was enhanced either by using growth interrupts at low growth temperatures or by growing at higher temperatures. Our observations are certainly consistent with this picture, as both growth interrupts and comparatively higher temperatures were employed.

Calculations of carrier transport through various heterostructures[7,30–32] have shown that scattering caused by interfacial roughness typically occurs for intermediate correlation lengths, on a length scale near the exciton radius, $\sim$10 nm in this system. Therefore, the impact of the short correlation lengths of our roughness on the device properties of this material is probably small, although calculations will be needed to verify the absolute magnitude of the effect. The next largest length scale in these materials is the terrace size, which at $>$50 nm is probably larger than the critical length scale for roughness-induced scattering. Therefore, the most appropriate model for understanding how the roughness of these interfaces affects the device properties is to treat each interface as a ''diffuse'' structure, $\sim$1-ML wide, having properties intermediate between those of InAs, InGaSb, and InSb.

B. Impurities and segregation effects

In addition to increased rms interfacial roughness with increasing temperature, we also observe degradation in the uniformity of the InGaSb alloy layer. There appears to be increased clustering, as revealed by XTEM (Fig. 5). This composition modulation is revealed by XTEM because of local variations in the elastic relaxation at the free surface caused by the varying lattice constant.[33] Similar variations can also be seen in XSTM images as shown in Fig. 6, where the uniformity of the optimal- and high-temperature samples is compared. By integrating the observed topographic height within the InGaSb layer along the growth direction, we find that clustering over a 5–10 nm length scale occurs much more strongly in the high-temperature sample. However, clustering in InGaSb is also evident in optimal samples, as seen in Fig. 7, where both the cation (empty states) and anion lattices (filled states) are shown together. (The clustering is clearest in the empty-state image.) This clustering will degrade the material properties in a manner similar to that of interfacial roughness. The observed clustering is most likely

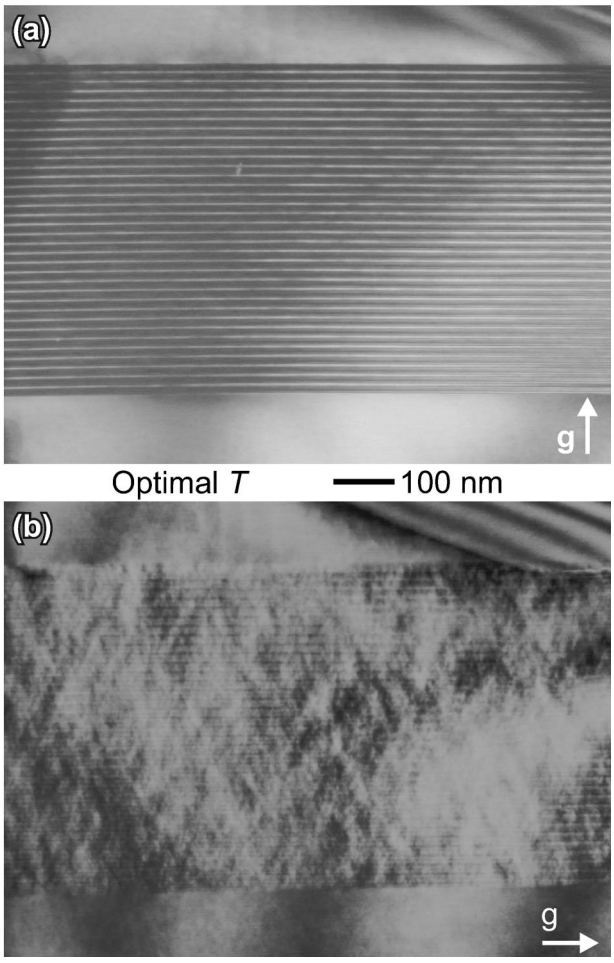

FIG. 5. Dark-field XTEM images of optimal temperature samples imaged using (a) a ⟨004⟩ refection and (b) a ⟨220⟩ reflection. Because the strain effects due to clustering are visible only using the latter imaging conditions, it is clear that composition undulations are parallel to the growth plane. The diffraction vector *g* is indicated.

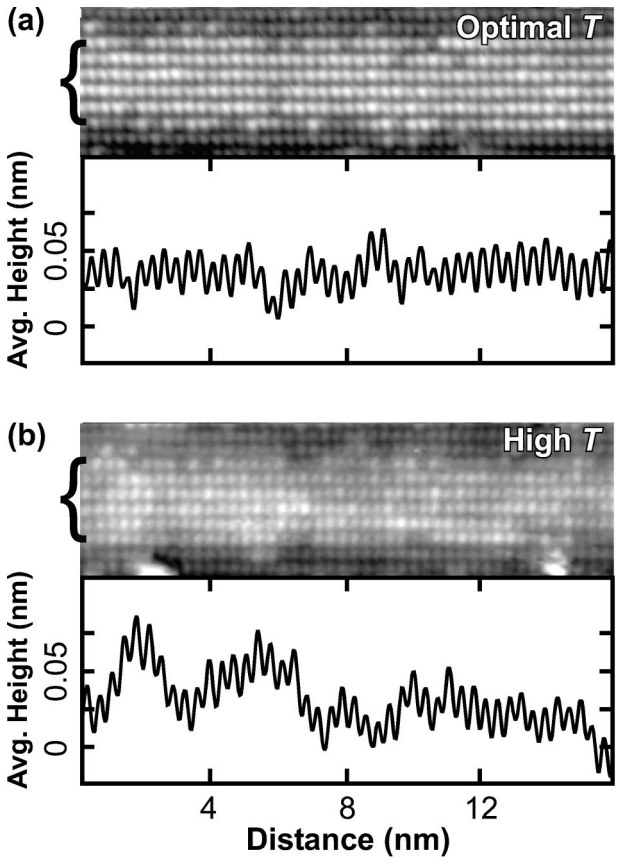

FIG. 6. XSTM images and average-height profiles for InGaSb-alloy layers in an (a) optimal- and (b) high-temperature sample. (a) −2.0 V, 50 pA and (b) −2.5 V, 0.5 nA.

thermodynamic in origin, being driven either by phase separation of InSb and GaSb or the well-known strain-driven instability predicted theoretically[34–36] and observed experimentally.[37] In either case, clustering should become increasingly manifest at higher temperatures when lateral segregation is less inhibited by the diffusion kinetics.

We find that several noteworthy defects occur even in the superlattices grown at the optimal temperature. As observed in Figs. 2(a), 7, and 8, the AlSb layers also exhibit some sort of contamination that appears as a series of topographically higher atoms in the XSTM, particularly near the AlSb-on-InAs interface. The most likely source of this contamination is In segregation into the AlSb layer associated with the MEE technique: each InAs layer was terminated with a monolayer of In, followed by an Sb soak to force this interface to be InSb-like. Other possible sources of contamination could be As from the interface, or the transient As background pressure, or excess Ga from the InGaSb floating on the surface of InAs.

In filled-state STM images of the {110} surfaces, one images only the anion sublattice, and image contrast primarily arises from two sources: anion identity and projected bond lengths perpendicular to the surface. It has been shown both experimentally[12,22] and theoretically[38] that the local III-V bond-length dominates the contrast for point defects. For example, As residing on a GaSb anion sublattice (a local ''GaAs'' defect) appears topographically lower than Sb,[19] so it is extremely unlikely that the source of the contrast is due to As cross contamination in the AlSb layer. If the observed features were due to misplaced cations in the AlSb, the local bond length would be slightly shorter for Ga, but longer for In (as observed). Similarly, we expect that local InSb structures should also appear topographically higher than both InAs and AlSb in empty-state images, as observed [Fig. 7(a)]. Therefore, we conclude that In contamination is the only type consistent with the XSTM contrast observed.

The In segregation creates discontinuous InSb layers up to about 4-ML thick sandwiched between the InAs and AlSb layers. The primary function of the AlSb layer is to separate out the superlattice periods to prevent the formation of undesirable extended three-dimensional electronic states between neighboring InAs layers. Therefore, this type of defect would not generally be expected to have a large impact on the electronic properties of the material. However, if the InSb layers locally perturb the symmetry of the superlattice, causing slightly different electron energy levels in the adjacent InAs layers, it could increase the width of the photoluminescence peak and reduce the total luminescence.

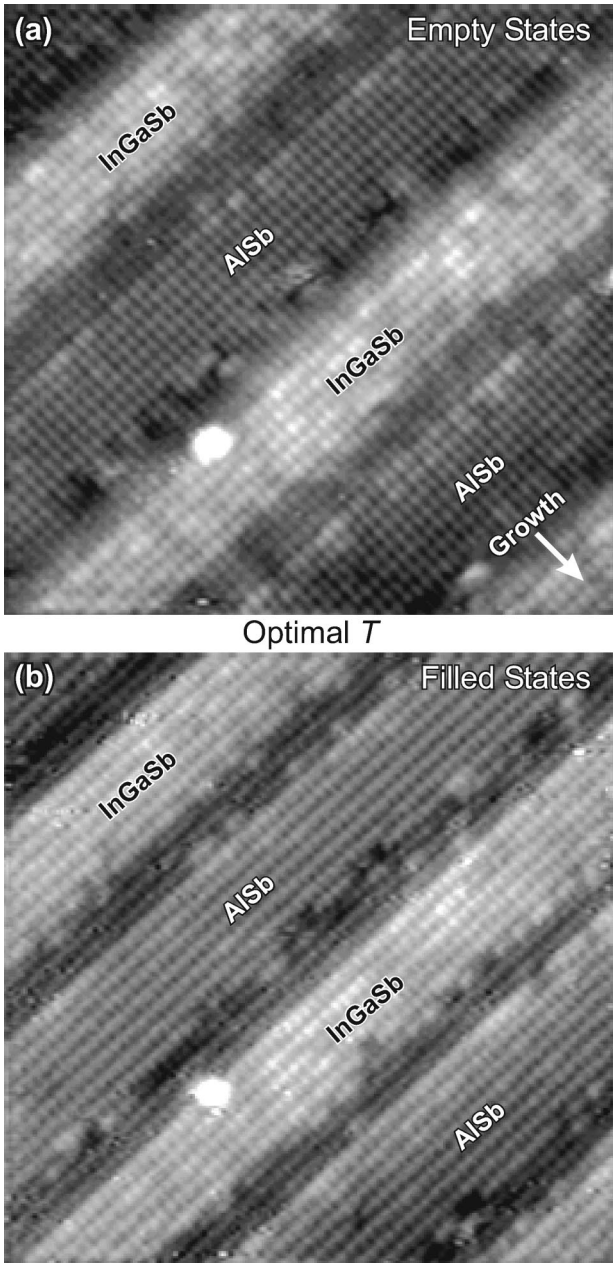

FIG. 7. XSTM images of optimal-temperature sample comparing simultaneously recorded (a) empty states (cation sublattice, +2.0 V, 50 pA) and (b) filled states (anion sublattice, −2.5 V, 50 pA).

C. Interfacial bonding

Another potential materials problem observed even in the optimal samples is the apparent growth-order dependence on the structure of the two InAs layers in each superlattice period. This asymmetry can be seen most clearly in Fig. 8. The first InAs layer in each ''W'' period tends to appear darker in filled-state gray-scale images than the second. Upon closer inspection, the source of this asymmetrical appearance is seen to be the structure of the InAs-AlSb interfaces. Whereas each InAs layer below AlSb has a relatively uniform appearance (gray arrows in the figure), the InAs layer above the

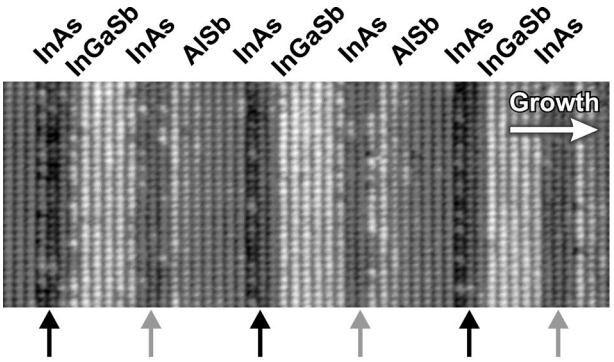

FIG. 8. XSTM image of multiple periods of an optimal-temperature sample highlighting the difference in the InAs layers when they are InAs-on-AlSb (dark arrows) vs AlSb-on-InAs (gray arrows). The image is of a (110) surface at −2.0 V, 50 pA.

AlSb on the top of each ''W'' has an InAs-on-AlSb interface that appears darker than the rest of the epilayer (black arrows). One mechanism for such contrast asymmetry between the two interfaces is different interfacial bond lengths normal to the surface associated with different interfacial bond types. For example, InAs-on-AlSb interfaces would appear topographically lower in the images if the interfacial bonds are AlAs rather than InSb as intended. An AlAs-like bond is significantly shorter than either an InAs or AlSb bond, and when oriented perpendicular to the surface, the terminal As atoms will be topographically lower than adjacent As surface atoms bonded to In. More detailed discussions of this effect can be found elsewhere.[12,22,38]

To help identify the interfacial bonds at the InAs-on-AlSb interfaces, we have grown two InAs/AlSb/InAs test heterostructures: the first with deliberately mixed As-Sb interfacial bonds and the second with uniform InSb bonds, prepared analogously to those in the laser structures. As previously reported, the appearance of interfacial bonds depends on the cleavage face examined, i.e., (110) vs $(\bar{1}\bar{1}0)$.[12,22] XSTM images of the mixed interfacial bonds indeed show topographically lower AlAs bonds at the InAs-on-AlSb interface on the (110) cleavage face [Fig. 9(a)] and at the AlSb-on-InAs interface on the $(\bar{1}\bar{1}0)$ face [Fig. 9(b)]. In principle, a similar examination of the different cleavage faces would elucidate the AlSb-on-InAs interfacial bonds in the laser structure samples. Because of the limited material available, we were unfortunately not able to image both cleavage faces on these samples, so we cannot definitively state whether AlAs interfacial bonds are present or not at the AlSb-on-InAs interfaces. However, given the presence of the In contamination in the AlSb layer (indicative of an In-rich, InSb interface), it is unlikely that AlAs bonding is significant at that interface.

The observation of AlAs-like interfacial bonds in the laser structures is very surprising given the growth procedures used. The 2-s Sb interrupt applied at each InAs-on-AlSb interface has been previously shown by x-ray superlattice diffraction to create an InSb-like interface.[39,40] To test the influence of interface formation techniques on the interfacial bond type, we grew the second test superlattice with nomi-

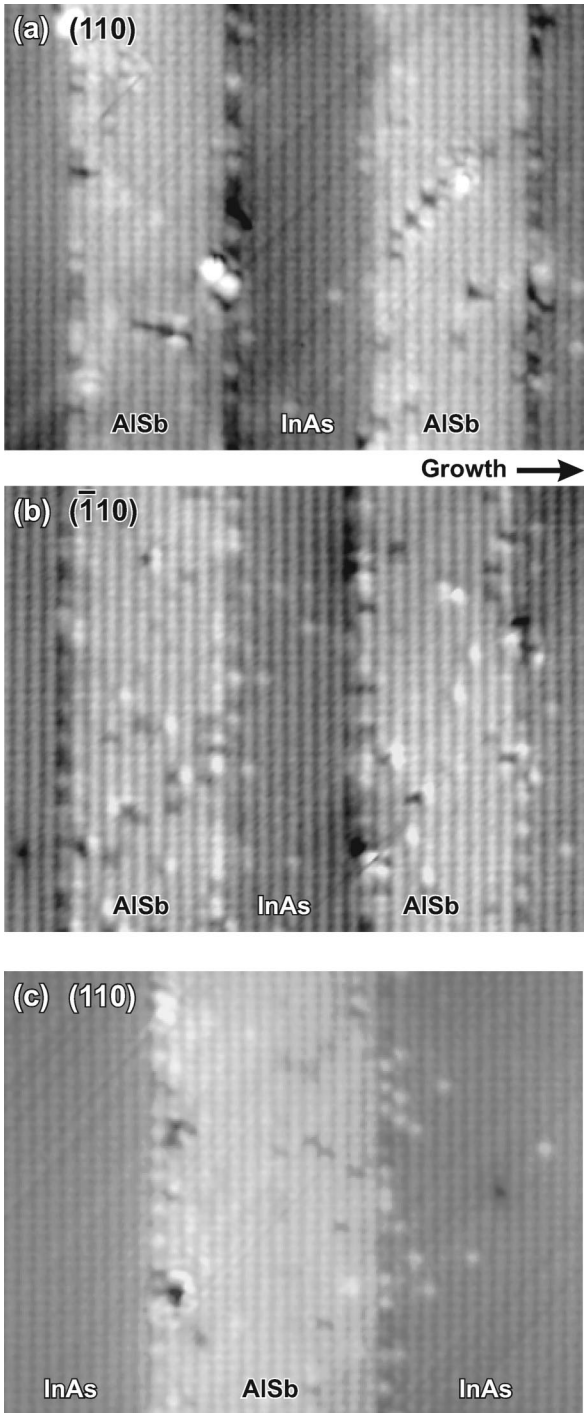

FIG. 9. XSTM image of InAs/AlSb superlattices grown with different interfacial bonds. (a) mixed AlAs/InSb interfacial bonds as seen on a (110) surface (−2 V, 0.1 nA). (b) The $(\bar{1}10)$ surface of the same superlattice (−3 V, 0.12 nA). (c) The (110) surface of a superlattice with InSb interfacial bonds grown using the same growth procedure nominally used for the laser structure samples (−2 V, 0.1 nA).

nally identical conditions and shutter sequences used to grow the optimized laser structures. Curiously, in these samples we do not see any evidence of anomalous AlAs interfacial bonds. In contrast to the laser structures, in these structures

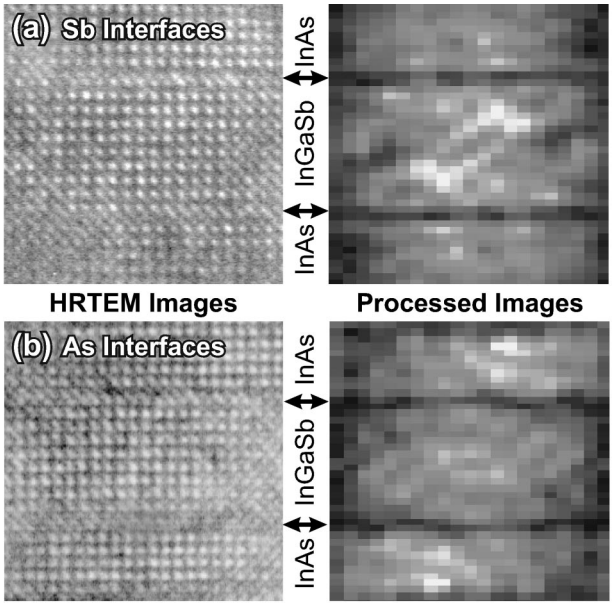

FIG. 10. High-resolution XTEM images (7×7 nm) of interfaces with (a) III-As and (b) III-Sb interfacial bonds. Images processed to reveal the composition-sensitive interface width are also shown (Ref. 14).

the interfacial bonds are InSb-like, as expected, appearing in the XSTM image [Fig. 9(c)] as a slightly raised row of Sb atoms along the AlSb/InAs interface. Similarly, in XSTM images of structures grown with shutter sequences intended to create AlAs interfacial bonds (not shown), a topographically lower row of As atoms is observed at each interface as expected. What is surprising is that the AlAs-like interfaces in that case look nearly the same as the InAs-on-AlSb interfaces in the laser structure (cf. Fig. 8), which were nominally grown with InSb interfacial bonds.

To date, we have been unable to determine why we observe this apparently anomalous interfacial bonding in the laser structures. However, the presence of such AlAs-like bonds at the InAs-on-AlSb interfaces would almost certainly be deleterious to the electronic quality of the material, degrading the performance of the device. Previous work has shown that As-like bonding is generally harmful for device material.[41] For instance, it drastically decreases the electron and hole mobility in AlSb/InAs/AlSb channels and increases the carrier concentration.[42] The decrease in carrier mobility has been attributed to increased interfacial roughness at AlAs-like interfaces,[43] although in our material the InAs-on-AlSb interfaces are not significantly rougher than the others (e.g., the InGaSb-on-InAs interfaces). The increased carrier density has been primarily attributed to a higher concentration of arsenic antisite defects near the interface.[44] In addition, the valence-band offsets have been shown to vary as a function of interfacial bond type, altering the electronic structure and further perturbing device performance.[45,46]

One alternate interpretation of the interfacial-bonding anomaly is that, in this case, we are incorrectly characterizing the ''dark'' rows as AlAs interfacial bonds. Perhaps the topography is caused by charge depletion at the InAs-on-AlSb interface, somehow associated with the asymmetrical

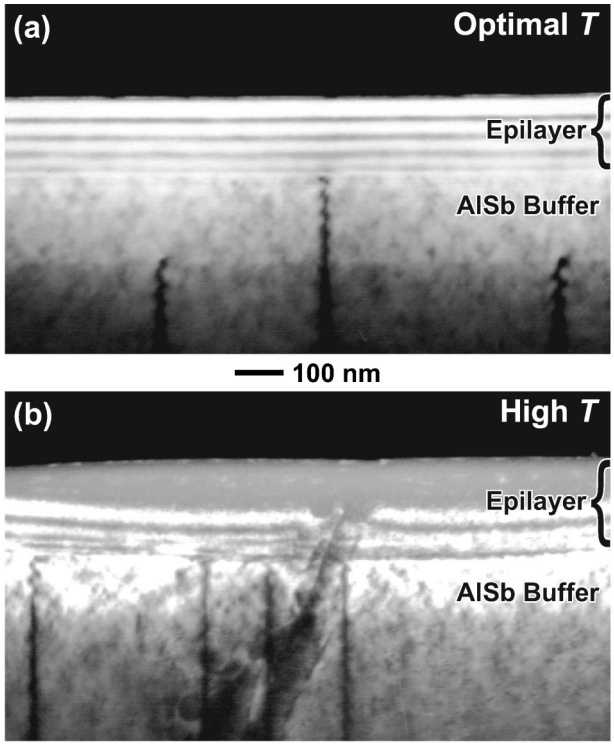

FIG. 11. Nearly plan-view TEM images of cleaved (a) optimal and (b) high-temperature samples. The samples were imaged through the cleaved edge of the sample. Misfit dislocations (which end at the cleave face between the substrate and epilayer) appear to terminate below the epilayer, whereas threading dislocations penetrate through the epilayer. The curved morphology of the cleaved edge in (b) may be due to strain effects.

InGaSb-on-thin InAs-on-AlSb structure. If this were the case, we might not see the same effect in simple (and thicker) AlSb/InAs superlattices. Clearly, resolution of this issue will require further investigation.

We have also used atomic-resolution HRTEM to investigate the structural quality of superlattice layers deliberately grown with Sb-like vs As-like interfacial bonds (Fig. 10). These samples had dramatically different optical properties, with the As-bonded samples exhibiting very low PL, even when grown at the optimal temperature (Fig. 1). After processing the HRTEM images to determine the interface width,[14] we find that the widths of the interfaces are the same in the two samples, 1.1–1.2 ML. In contrast to previous assertions,[43] in our samples we see no evidence that the III-As-like interfaces are rougher than the InSb-like ones. It is possible that there are differences in the structure of these interfaces at longer length scales, but the limited (10–20)-nm lateral field of view for cleaved HRTEM samples of optimal thickness makes this difficult for us to determine. However, XTEM observations indicate that both samples have dislocation densities $<10^7/\mathrm{cm}^{-2}$. Therefore, we conclude that the degradation in PL associated with III-As interfacial bonds is primarily an optoelectronic effect of the bond type.

D. Meso-scale defects

We find that one additional source of material degradation originates at the mesoscale. As illustrated in Fig. 11, epilayers grown in the optimum temperature range appear defect-free in plan-view TEM images of cleaved samples, with the misfit dislocations ($<10^5\ \mathrm{cm}^{-2}$)—caused by the AlSb buffer layer/GaSb substrate lattice mismatch (0.66%)—confined to the buffer layer. In contrast, in samples grown at higher temperature, the dislocations ($>10^6\ \mathrm{cm}^{-2}$) thread through the epilayers, suggesting that the growth temperature exceeded the elastic-plastic transition for some of the components in the superlattice. Although the presence of these dislocations is almost certainly deleterious to device performance, their role in the PL degradation is unclear. The electron and hole pairs that recombine to produce the measured photons are believed to migrate $\leqslant 1\ \mu$m from the position where they were generated before recombining, a distance somewhat shorter than the typical threading dislocation separation. Therefore, it would be very surprising if the threading dislocations are primarily responsible for the dramatic reduction in PL intensity. However, we have identified no other compelling sources of material degradation that would account for the PL data.

IV. SUMMARY

We have used XSTM and TEM to investigate the structural quality of several InAs/$In_{0.28}Ga_{0.73}$Sb/InAs/AlSb strained-layer heterostructures as a function of growth temperature (optimal vs high) and interfacial bond type (III-Sb vs III-As). Implementing various methods for characterizing interfacial roughness, we find that the roughness at the crucial InAs/InGaSb interfaces is generally larger for the higher growth temperature. We deduce from the surprisingly short correlation length of the interface profiles that the primary source of the roughening is most likely a direct result of the MEE technique used to form the interfaces. Even samples grown at the optimum temperature show significant In intermixing at the AlSb-on-InAs interfaces. This intermixing is accompanied by anomalous AlAs bonding at the InAs-on-AlSb interfaces; surprisingly, neither the intermixing nor the AlAs bonding is observed in InAs/AlSb test structures grown under nominally identical conditions. We find that the primary source of material degradation in layers grown at the high temperature appears to be threading dislocations that propagate from the substrate-epilayer interface through the heterostructure.

This work highlights how XSTM and TEM can be applied in a complementary fashion to characterize III-V heterostructures over a range of length scales. In particular, when XSTM is performed on a {110} cleavage surface, the *same samples* of superlattice material can be analyzed using both techniques. The atomic and nanoscale structures (including point defects) are captured using XSTM, and the sparser mesoscale structures (such as dislocations and precipitates) can be easily identified using TEM. Although im-

aging of individual atomic columns is straightforward in HR-TEM, the actual imaging of individual atoms (at least in the cross-sectional samples discussed here) is only achievable in XSTM. Accordingly, for samples that can be easily cleaved in vacuum, XSTM provides a more complete analysis, especially if detailed quantitative roughness spectra are of interest.

ACKNOWLEDGMENTS

This work was supported by the Office of Naval Research, the Air Force Research Laboratory, and an NRC/NRL Postdoctoral Research Associateship (WB-C). We also thank Dr. B. Z. Nosho and Dr. J. R. Meyer for helpful discussions.

*Present address: HRL Laboratories, 3011 Malibu Canyon Rd., Malibu, CA 90265.

†Corresponding author. Email address: lloyd.whitman@nrl.navy.mil

[1] G. W. Turner and H. K. Choi, in *Optoelectronic Properties of Semiconductors and Superlattices*, edited by M. O. Manasreh (Gordon and Breach, New York, 1997), Vol. 3.

[2] B. V. Shanabrook, W. Barvosa-Carter, R. Bass, B. R. Bennett, J. B. Boos, W. W. Bewley, A. S. Bracker, J. C. Culbertson, E. R. Glaser, W. Kruppa, R. Magno, W. J. Moore, J. R. Meyer, B. Z. Nosho, D. Park, P. M. Thibado, M. E. Twigg, R. J. Wagner, J. R. Waterman, L. J. Whitman, and M. J. Yang, Proc. SPIE **3790**, 13 (1999).

[3] F. Capasso, C. Gmachl, D. L. Sivco, and A. Y. Cho, Phys. World **12**, 27 (1999).

[4] J. I. Malin, J. R. Meyer, C. L. Felix, J. R. Lindle, L. Goldberg, C. A. Hoffman, F. J. Bartoli, C. H. Lin, P. C. Chang, S. J. Murry, R. Q. Yang, and S. S. Pei, Appl. Phys. Lett. **68**, 2976 (1996).

[5] W. W. Bewley, C. L. Felix, I. Vurgaftman, D. W. Stokes, E. H. Aifer, L. J. Olafsen, J. R. Meyer, M. J. Yang, B. V. Shanabrook, H. Lee, R. U. Martinelli, and A. R. Sugg, Appl. Phys. Lett. **74**, 1075 (1999).

[6] F. Capasso, A. Tredicucci, C. Gmachl, D. L. Sivco, A. L. Hutchinson, A. Y. Cho, and G. Scamarcio, IEEE J. Sel. Top. Quantum Electron. **5**, 792 (1999).

[7] D. Y. Ting and T. C. McGill, J. Vac. Sci. Technol. B **14**, 2790 (1996).

[8] G. Klimeck, R. Lake, and D. K. Blanks, Phys. Rev. B **58**, 7279 (1998).

[9] J. R. Meyer, C. A. Hoffman, F. J. Bartoli, and L. R. Ram Mohan, Appl. Phys. Lett. **67**, 757 (1995).

[10] M. J. Yang, W. J. Moore, B. R. Bennett, and B. V. Shanabrook, Electron. Lett. **34**, 270 (1998).

[11] M. J. Yang, W. J. Moore, B. R. Bennett, B. V. Shanabrook, J. O. Cross, W. W. Bewley, C. L. Felix, I. Vurgaftman, and J. R. Meyer, J. Appl. Phys. **86**, 1796 (1999).

[12] B. Z. Nosho, W. Barvosa-Carter, M. J. Yang, B. R. Bennett, and L. J. Whitman, Surf. Sci. **465**, 361 (2000).

[13] M. J. Yang, W. J. Moore, C. H. Yang, R. A. Wilson, B. R. Bennett, and B. V. Shanabrook, J. Appl. Phys. **85**, 6632 (1999).

[14] M. E. Twigg, B. R. Bennett, P. M. Thibado, B. V. Shanabrook, and L. J. Whitman, Philos. Mag. A **77**, 7 (1998).

[15] R. M. Feenstra, D. A. Collins, and T. C. McGill, Superlattices Microstruct. **15**, 215 (1994).

[16] R. M. Feenstra, D. A. Collins, D. Y. Ting, M. W. Wang, and T. C. McGill, Phys. Rev. Lett. **72**, 2749 (1994).

[17] R. M. Feenstra, D. A. Collins, D. Y. Ting, M. W. Wang, and T. C. McGill, J. Vac. Sci. Technol. B **12**, 2592 (1994).

[18] J. Harper, M. Weimer, D. Zhang, C. H. Lin, and S. S. Pei, Appl. Phys. Lett. **73**, 2805 (1998).

[19] J. Harper, M. Weimer, D. Zhang, C. H. Lin, and S. S. Pei, J. Vac. Sci. Technol. B **16**, 1389 (1998).

[20] M. B. Johnson, U. Maier, H. P. Meier, and H. W. M. Salemink, Appl. Phys. Lett. **63**, 1273 (1993).

[21] H. W. M. Salemink, M. B. Johnson, and O. Albrektsen, J. Vac. Sci. Technol. B **12**, 362 (1994).

[22] J. Steinshnider, M. Weimer, R. Kaspi, and G. W. Turner, Phys. Rev. Lett. **85**, 2953 (2000).

[23] Similarly, the values of the actual autocorrelation function for the interface profile can be obtained from an autocorrelation of the oversampled interface data by summation around the nearest-neighbor positions.

[24] It is important to note that our results do not depend on this short sampling length. We obtain nearly identical results (but with correspondingly poorer statistics) using a subset of the profiles that are either two or three times longer.

[25] W. H. Press, S. A. Teukolksky, W. T. Vetterling, and B. P. Flannery, *Numerical Recipes in C*, 2nd ed. (Cambridge University Press, Cambridge, 1992).

[26] A. Y. Lew, S. L. Zuo, E. T. Yu, and R. H. Miles, Phys. Rev. B **57**, 6534 (1998).

[27] B. Z. Nosho, W. H. Weinberg, W. Barvosa-Carter, A. S. Bracker, R. Magno, B. R. Bennett, J. C. Culbertson, B. V. Shanabrook, and L. J. Whitman, J. Vac. Sci. Technol. B **17**, 1786 (1999).

[28] B. Z. Nosho, W. H. Weinberg, W. Barvosa-Carter, B. R. Bennett, B. V. Shanabrook, and L. J. Whitman, Appl. Phys. Lett. **74**, 1704 (1999).

[29] J. Steinshnider, J. Harper, M. Weimer, C. H. Lin, S. S. Pei, and D. H. Chow, Phys. Rev. Lett. **85**, 4562 (2000).

[30] D. Y. Ting, Microelectron. J. **30**, 985 (1999).

[31] M. J. Shaw, J. P. Hagon, E. A. Corbin, and M. Jaros, J. Vac. Sci. Technol. B **17**, 2025 (1999).

[32] M. J. Shaw, E. A. Corbin, M. R. Kitchin, J. P. Hagon, and M. Jaros, J. Vac. Sci. Technol. B **18**, 2088 (2000).

[33] M. M. J. Treacy, J. M. Gibson, and A. Howie, Philos. Mag. A **51**, 389 (1985).

[34] B. J. Spencer, P. W. Voorhees, and S. H. Davis, J. Appl. Phys. **73**, 4955 (1993).

[35] J. E. Guyer and P. W. Voorhees, Phys. Rev. B **54**, 11 710 (1996).

[36] B. J. Spencer, P. W. Voorhees, and J. Tersoff, Phys. Rev. Lett. **84**, 2449 (2000).

[37] M. E. Twigg, B. R. Bennett, and R. Magno, J. Cryst. Growth **191**, 651 (1998).

[38] S.-G. Kim, B. Z. Nosho, L. J. Whitman, and S. C. Erwin (unpublished).

[39] B. R. Bennett, B. V. Shanabrook, R. J. Wagner, J. L. Davis, and J. R. Waterman, Appl. Phys. Lett. **63**, 949 (1993).

[40] B. R. Bennett, B. V. Shanabrook, and M. E. Twigg, J. Appl. Phys. **85**, 2157 (1999).

[41] J. R. Waterman, B. V. Shanabrook, R. J. Wagner, M. J. Yang, J.

L. Davis, and J. P. Omaggio, Semicond. Sci. Technol. **8**, S106 (1993).
[42] G. Tuttle, H. Kroemer, and J. H. English, J. Appl. Phys. **67**, 3032 (1990).
[43] K. C. Wong, C. Yang, M. Thomas, and H. R. Blank, J. Appl. Phys. **82**, 4904 (1997).
[44] J. Shen, H. Goronkin, J. D. Dow, and R. Shang Yuan, J. Vac. Sci. Technol. B **13**, 1736 (1995).
[45] E. R. Glaser, T. A. Kennedy, B. R. Bennett, B. V. Shanabrook, L. A. Hemstreet, M. W. Bayerl, and M. S. Brandt, Physica B **273**, 811 (1999).
[46] E. R. Glaser, T. A. Kennedy, B. R. Bennett, and B. V. Shanabrook, Phys. Rev. B **59**, 2240 (1999).